Optical absorption and photoluminescence properties of a-$Si_{1-x}N_x$:H films deposited by plasma-enhanced CVD

F. Giorgis
INFM and Physics Department, Polytechnic of Torino, C.so, Duca degli Abruzzi 24, 10129 Torino, Italy

C. Vinegoni and L. Pavesi
INFM and Physics Department, University of Trento, Via Sommarive 14, 38050 Povo, Italy
(Received 13 May 1999)

Optical absorption and photoluminescence (PL) measurements were performed on a series of hydrogenated silicon-nitrogen thin films deposited by plasma enhanced chemical vapor deposition covering a wide compositional range with the aim to find how absorption and emission processes are correlated. Our analysis indicates that the observed broadening of the PL spectra is linked with the existence of band tail states due to topological disorder, as confirmed by the spectral dependence of the PL decay. Moreover, nitrogen alloying reduces the temperature quenching of luminescence and increases the radiative recombination rate. Such phenomena are ascribed to the formation of wide tails in the density of states of N-rich samples and, in turn, to a lower carrier diffusion.

I. INTRODUCTION

Hydrogenated amorphous silicon nitrogen alloys (a-$Si_{1-x}N_x$:H) deposited by plasma enhanced chemical vapor deposition (PECVD) have been extensively used for a wide variety of microelectronic and optoelectronic applications such as passivation layers for device packaging,[1] gate dielectric in a-Si:H thin-film transistors,[2] charge storage layers in MNOS nonvolatile memories, hot-carrier injection layers,[3] and radiative elements in light-emitting devices both in homogeneous[4] and in multilayered structures.[5] Such alloy presents the peculiarity to have an optical gap tunable from 1.9 up to 5 eV, depending on nitrogen content.[6] At the same time, by increasing nitrogen content, the radiative efficiency at room temperature is enhanced by several orders of magnitude and the emission band is shifted towards higher energies, thus making silicon-nitrogen alloys very appealing for light-emission applications. Early studies established some relevant features of a-$Si_{1-x}N_x$:H photoluminescence (PL) properties.[7,8] On the other hand, there is a lack of information about the carrier recombination kinetics and only few analysis of time-resolved photoluminescence were reported.[9,10] In this paper, the optical properties of a-$Si_{1-x}N_x$:H samples with x ranging from 0.15 up to 0.52 are investigated by transmittance-reflectance (T-R), photothermal deflection spectroscopies (PDS), stationary, and time-resolved photoluminescence measurements. Such techniques allow us to link the most relevant emission features, such as the PL band-shape and the lifetime distribution, to the electronic density of states (DOS) and to get an insight on the radiative and nonradiative processes for the wide compositional range here investigated.

II. SAMPLES AND EXPERIMENTAL DETAILS

All the samples were deposited by a 13.56 MHz PECVD system on (100) Si wafers, 7059 Corning glass and quarz substrates. The films were grown in SiH_4+NH_3 gas mixtures by changing the ammonia percentage in the plasma $[NH_3]/[SiH_4+NH_3]$ in the range $13\%\div 90\%$, with and without hydrogen dilution with a percentage $[H_2]/[SiH_4+NH_3+H_2]$ of 93% and a total gas flow in the range of $7.5\div 110$ sccm. The other deposition conditions, determined by optimizing the film uniformity and optoelectronic properties were: substrate temperature of 220 °C, pressure of 0.8–0.9 bar, a delivered r.f. power of 4 W, an electrode area and distance of 144 cm^2 and 20 mm, respectively. The sample thicknesses were in the range of $0.5\div 4$ μm. The determination of silicon and nitrogen contents was performed by Rutherford-back-scattering (RBS) technique with alpha particles of 1.8 MeV. Optical absorption characterizations were performed by T-R measurement in the range of 200–1500 nm with a grating dispersive spectrophotometer and by PDS technique in the range of 440-1100 nm with a conventional experimental set-up where carbon tetrachloride (CCl_4) was the deflecting medium for the probe beam, which was an He-Ne laser. Continuous wave photoluminescence measurements (CW PL) were performed at temperature ranging from 77 up to 300 K, using a f/4 monochromator, an Ar^+ laser or a Xe-Hg lamp as exciting sources (line at 2.71 and 3.4 eV, respectively), and a c-Si photodiode whose signal was processed by a digital lock-in amplifier. Time-resolved photoluminescence measurements (TRL) were performed by using a mode-locked frequency-doubled Ti:Sapphire laser as pulsed excitation source (pulse duration 2 ps, wavelength 390 nm, repetition frequency 4 MHz). A single monochromator coupled to a streak-camera directly interfaced to a computer was used for the recording of two dimensional (time and wavelength) luminescence maps.

III. RESULTS

The elemental composition of all the examined a-$Si_{1-x}N_x$:H has been determined by RBS, revealing a good uniformity of nitrogen and silicon profile. What is observed is a fairly linear trend of N incorporation with respect

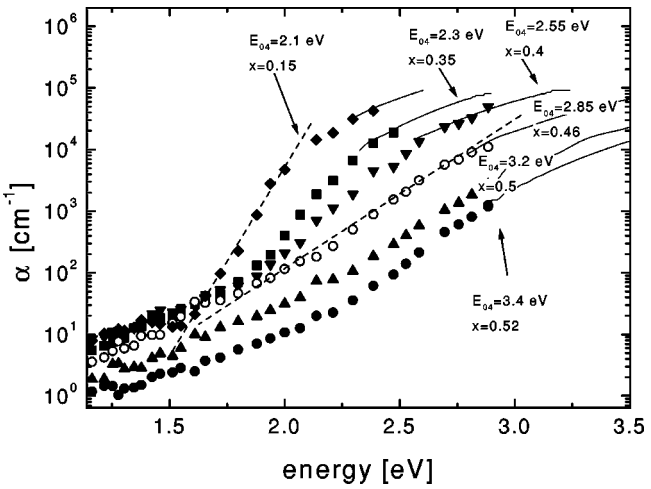

FIG. 1. Absorption coefficient distribution for a-$Si_{1-x}N_x$:H films with different atomic composition, the continuous lines and the symbols represent the T-R and PDS data, respectively. The composition and the optical gap are indicated for each curve. Exponential fits in the Urbach region are shown as dashed lines for two different samples. From fits of this kind, the Urbach energies were derived for all samples.

to the N content in the plasma, in agreement with other findings concerning silicon nitride thin films grown by 13.56 MHz PECVD.[6,7] T-R and PDS spectroscopies applied to samples with different stoichiometry allows to extract the absorption distribution in a wide energy range reported in Fig. 1. We define the optical gap E_{04} as the energy for which the absorption coefficient $\alpha = 10^4$ cm^{-1}. It is straighforward to observe that N incorporation causes a monotonical enhancement of the optical gap. Moreover, for Si-rich materials we can distinguish three typical regions: (a) the fundamental absorption region (high energy), (b) the exponential tail region (intermediate energy), mainly due to static disorder, characterized by the Urbach energy (E_U), namely the logarithmic slope of the absorption distribution for which $\alpha \sim \exp(E/E_U)$, and (c) the excess absorption region (low energy). When the N content increases, E_U increases, and these three features remain with a less marked demarcation energy.

Figure 2 shows typical CW PL spectra at 77 K of a-$Si_{1-x}N_x$:H samples. All the samples have been excited at energies higher than E_{04} in order to avoid any modifications of emission energy (E_L) and full width at half maximum (ΔE_L), which is known to occur for longer excitation wavelengths. The PL emission band is gaussian-like for all the

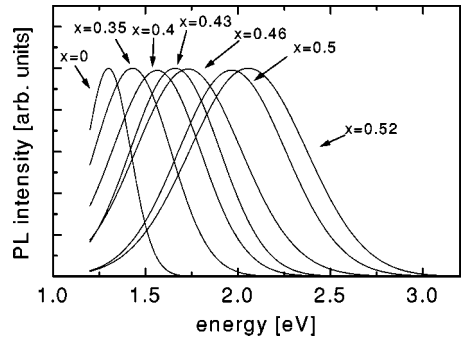

FIG. 2. Normalized PL spectra taken at 77 K.

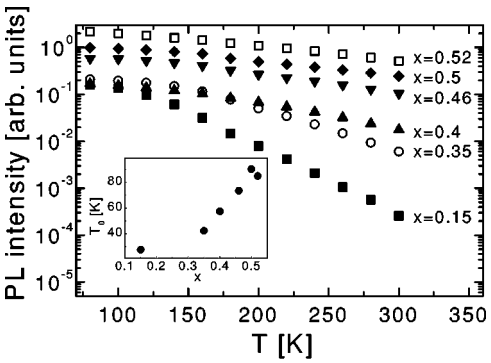

FIG. 3. PL efficiency versus temperature for different samples. The efficiencies are extracted by the intensity of the integrated PL spectra normalized to the samples' absorption at the excitation energy. The inset shows the variation of the T_0 parameter versus composition x (see text).

samples. As the N content increases two systematic trends can be observed: (i) the PL spectra shift toward higher energies and (ii) they get broader, in agreement with the findings of other groups.[7]

The alloying strongly modifies also the temperature dependence of the PL intensity. Figure 3 shows the luminescence efficiency of several samples as a function of T in the range 77-300 K. Such efficiencies were obtained by normalizing the integrated PL spectra for the sample absorbance at the excitation wavelength, avoiding with care any specimen misalignment. The temperature quenching of the PL is weakened by alloying. In particular, the room-temperature luminescence efficiency increases by several order of magnitude by increasing x.

Finally, time-resolved luminescence measurements have been performed at 77 K on some samples by monitoring the luminescence decay at different emission energy E_{em}. Fast decays are observed for a-$Si_{1-x}N_x$:H samples with different stoichiometry. The luminescence decay lineshapes follow a stretched-exponential law

$$I(t) = I_0 \exp[-(t/\tau)^{\beta}], \tag{1}$$

where $I(t)$ is the luminescence intensity at time t, τ is the decay lifetime, and β is a dispersion exponent. Figure 4(a) shows a typical PL decays for an a-$Si_{0.6}N_{0.4}$:H sample at several E_{em} with the respective stretched exponential fits. To discuss the experimental data, we consider the time dependent PL intensity $I(t)$ to be composed of an infinite number of pure exponentials weighted by a decay rate distribution $G(\tau)/\tau$ (Ref. 11)

$$I(t) \propto \int_0^{\infty} \frac{G(\tau)}{\tau} \exp\left(-\frac{t}{\tau}\right) d\tau. \tag{2}$$

With the β and τ parameters obtained by least square fits of data, an asymptotic function has been used to estimate the distribution $G(\tau)$ (Ref. 12) and an average decay time has been calculated as:

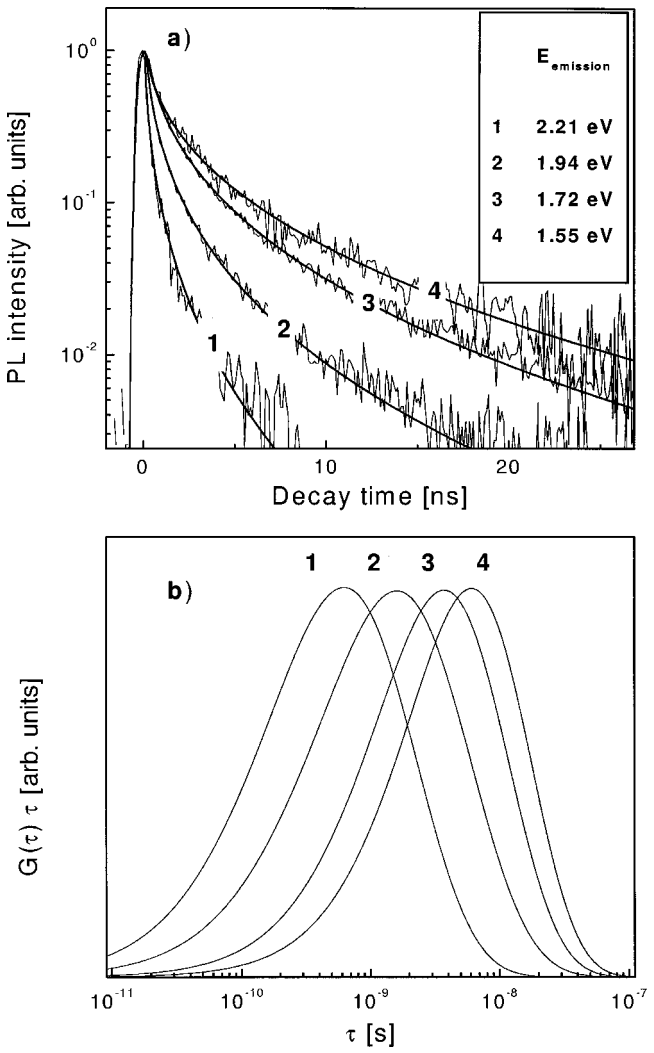

FIG. 4. (a) Typical time resolved photoluminescence at $T=77$ K for a a-$Si_{0.6}N_{0.4}$:H film. The spectra at several emission energy (E_{em}) are reported. The smooth curves show the results of the best fit using the stretched-exponential function. The luminescence is integrated over a wavelength interval 90 nm large. (b) Distribution of decay times $G(\tau)$ calculated for the corrisponding E_{em}. Here, $\tau\, G(\tau)$ is plotted to account for the logarithmic time scale.

$$\overline{\tau}=\frac{\int_0^\infty \tau G(\tau)d\tau}{\int_0^\infty G(\tau)d\tau}. \tag{3}$$

The decay times distribution $G(\tau)$ calculated by the PL decays of the a-$Si_{0.6}N_{0.4}$:H sample are shown in Fig. 4(b).

In Fig. 5, $\overline{\tau}$ is plotted versus E_{em} for two different samples. An exponential dependence $\exp(-E_{em}/\gamma)$ is found with the γ parameter increasing as x increases.

IV. DISCUSSION

Let us start with the discussion of the optical properties of the analyzed a-$Si_{1-x}N_x$:H samples focussing on their absorption (Fig. 1). Like for a-Si:H, some groups[13] tried to decompose PDS spectra of silicon nitride films into a weak

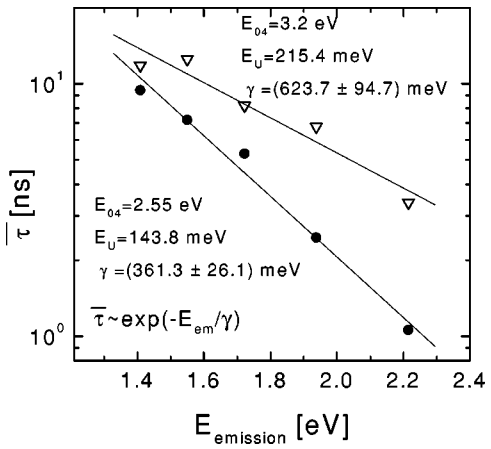

FIG. 5. Average decay time versus detection energy for two different samples. The respective sample optical gap E_{04}, Urbach energy E_U and γ values obtained by the best exponential fits (continuous lines) are indicated.

absorption region (ascribed to defects-extended states transitions) and an exponential absorption region (ascribed to tail states-extended states transitions). The first region extends to energies lower than half of the optical gap, where the existence of Si dangling bonds is plausible. It is worth to emphasize that in homogeneous amorphous semiconductors such as a-Si:H, electronic transitions between localized states must be excluded because of a too small optical matrix element for transition between spatially correlated states. Assuming that from a microscopic point of view, a-$Si_{1-x}N_x$:H is a compositionally heterogeneous material with spatial bandgap fluctuations,[14] the localized states are spatially correlated allowing also optical transitions between states lying in the suboptical gap region. Morover, a noticeable spread of the Si dangling bonds levels could be expected due to the gap center fluctuations and to the variation of defect levels relative to each local gap center. These effects could account for the observed features in absorption at low energies. Regarding the exponential absorption region, we can assume that the Urbach energy increase with alloying follows the broadening of the tail states distribution. Moreover, taking into account that the Urbach edge and the bandgap transitions of different regions could overlap, large E_U for samples with high N content were expected and indeed measured.

To investigate the correlation between the absorption and the emission data, we consider two main models: the Stokes-shift and the static disorder models. The first one assumes that the electron- phonon coupling originates both the shift of the emission energy with respect to the optical gap and the PL broadening. The second one ascribes the PL line shape to the band tail states distribution.

It has to be pointed out that, for the following study, E_{04} and E_U has been measured at room temperature, while E_L and ΔE_L were taken at 77 K. This fact does not affect the analysis since in a-Si:H both the optical gap and Urbach energy are weakly influenced by temperature in the range 77-300 K (ΔE_{04}[77 K$\rightarrow$300 K]$\approx$2.6%, ΔE_U[77 K$\rightarrow$300 K]$\approx$15%).[15] In a-$Si_{1-x}N_x$:H alloy, it is arguable a weaker temperature dependance due to the enhanced topological disorder.

The Stokes-shift model has been deeply studied in

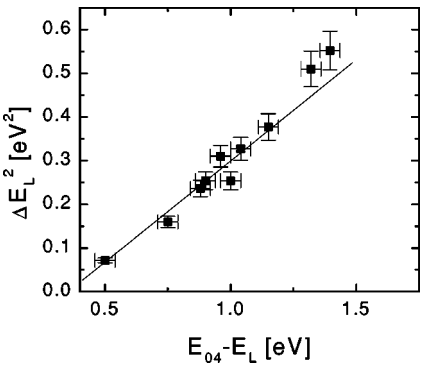

FIG. 6. Squared PL linewidth versus PL peak separation from the optical gap $E_{04}-E_L$, taken for a-$Si_{1-x}N_x$:H samples with $0 \leqslant x \leqslant 0.52$. The straight line show the best linear fit with slope 0.463 eV.

crystals[16] and its predictions seem well consolidated. ΔE_L and the dominant phonon energy $\hbar\omega_{ph}$ are correlated by

$$(\Delta E_L)^2 = 4\ln(2) E_S \hbar\omega_{ph}, \tag{4}$$

where $E_S = E_A - E_L$ and E_A is the peak energy of the absorption band. For amorphous semiconductors, Eq. (4) has to be corrected by a term E_{th} that accounts for the carrier thermalization in the tail states. By imposing $E_A = E_{04}$ and by considering an extra-broadening due to static disorder ΔE_L^{STAT},

$$(\Delta E_L)^2 = 4\ln(2)(E_{04} - E_L - E_{th})\hbar\omega_{ph} + (\Delta E_L^{STAT})^2. \tag{5}$$

Figure 6 shows that the measured $(\Delta E_L)^2$ vs $(E_{04}-E_L)$ is in agreement with Eq. (4). The best linear fit yields a slope of (0.463 ± 0.028) eV and a zero intercept of (-0.164 ± 0.019) eV^2 with a correlation coefficient R=0.986. However, from the slope of the plot $\hbar\omega_{ph} = 167$ meV is obtained, a value too high for a typical phonon energy in amorphous silicon-based alloys. In fact, in a-Si:H the dominant phonon energy is about 60 meV, as can be experimentally verified by Raman spectroscopy.[17] Moreover, the extracted thermalization energy by the zero intercept is $E_{th} = 352$ meV when $\Delta E_L^{STAT} = 0$. Such a value is much higher than the ΔE_L of a typical a-Si:H PL spectrum. In summary, such results evidence that in our case the Stokes-shift model fails.

Let us consider the static disorder model, within the Dunstain and Boulitrop theory.[18,19] The PL line shape is due to the photogenerated carrier distribution in the exponential band tail density of states available for radiative recombination. After a fast thermalization to the band edges, holes, and electrons start a slower thermalization in the tails. The radiative recombination happens when the carriers reach the deepest states within spheres with a critical radius R_C, namely the carrier-tail state for which the radiative recombination and thermalization rates are equal, given by[18]

$$R_C = \frac{R_e}{2}\ln(\omega_0 \tau_R), \tag{6}$$

where R_e is the localization length of the electron, ω_0 is a typical acoustic-phonon frequency and τ_R is the radiative lifetime.

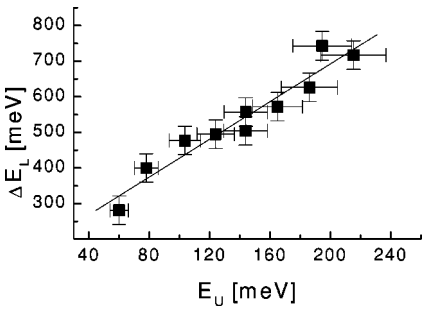

FIG. 7. PL linewidth ΔE_L versus Urbach energy E_U for the samples analyzed in Fig. 6. The slope of the linear best fit is 2.64.

Supposing that the tail states are distributed randomly in space but exponentially in energy (with logarithmic slope E_0), and that R_C is a constant, the density of such states is described by

$$P_X(E) \propto \exp\left(-\frac{E}{E_0^X}\right)\exp\left[-\frac{4}{3}\pi R_C^3 N_0^X E_0^X \exp\left(-\frac{E}{E_0^X}\right)\right], \tag{7}$$

where $X = e,h$ is an index indicating the electron or hole distribution, N_0 is the DOS at the band edge, and E is measured from the mobility edge. The PL spectrum strictly depends upon the P_e and P_h convolution. Thus, when the slope of the valence tail is higher than that of the conduction one, ΔE_L is linked to the former slope. E_0 can be identified with the Urbach energy extracted by PDS measurement. Hence, from this identification it follows

$$\Delta E_L = \xi E_U, \quad \text{where} \quad \xi = 2.45. \tag{8}$$

ξ is independent on R_C. Moreover, it is straightforward to demonstrate from Eq. (7) that the shift of the PL peak with respect to the optical gap is given by

$$E_{04} - E_L = E_U \ln(\tfrac{4}{3}\pi R_C^3 N_0 E_U). \tag{9}$$

In addition, considering also electron-phonon coupling effects, Eq. (4) becomes

$$(\Delta E_L)^2 = (\xi E_U)^2 + (\Delta E_L^{e-ph})^2. \tag{10}$$

PL analysis of amorphous silicon based alloys found $\xi > 2.45$. For instance, for tethraedrally coordinated a-SiC:H alloy it was found $\xi = 3.85$.[20] Such large value of ξ has been explained by the fact that absorption is sensitive only to antiparallel potential fluctuations while radiative recombination follows a thermalization process where the carriers can span tail states related to both parallel and antiparallel fluctuations.[20] Hence, the slope of the tail density of states probed by the luminescence process is understimated by optical characterization through the Urbach energy. The Sheffield's group found a slope of 4.4 for a-$Si_{1-x}N_x$:H,[8] however, they analyzed only one sample with high-N content (say with optical gap higher than 2.5 eV). In the present paper, several samples have optical gap in the range 2.5 eV-3.4 eV, making the analysis more reliable.

Figure 7 represents ΔE_L versus E_U for our samples. The slope of the best linear fit is 2.64 ± 0.25, with R=0.965, that

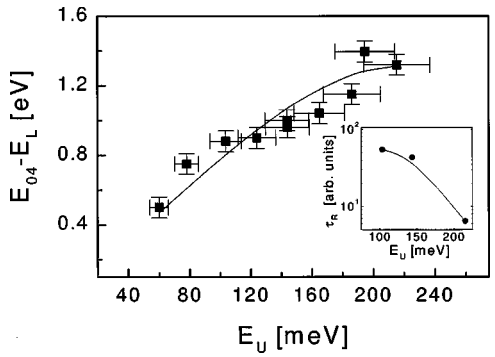

FIG. 8. $E_{04}-E_L$ versus E_U for a-$Si_{1-x}N_x$:H films with several compositions. The line shows the calculation by applying Eq. (9), where a linear decrease of R_C vs E_U, from 125 to 46 Å is imposed. The inset shows the trend of the radiative lifetime vs E_U (line is drawn as guides for the eyes).

accounts quite well for the trend predicted by the static disorder model. On the other hand the zero intercept is (163 $\pm$38) meV. Such a value could be justified by the presence of the electron-phonon coupling, which however does not represent the dominant process. In fact, assuming $\hbar\omega_{ph}$ =60 meV, it is straightforward from Eq. (4) to obtain a Stokes shift E_S=160 meV, a value too low to justify electron-phonon disorder as the only cause of the PL bandwidth even for a-Si:H.

In order to deepen the analysis of the static disorder model, we check also the validity of Eq. (9), by plotting in Fig. 8 the PL peak separation from the gap $E_{04}-E_L$ versus E_U. In our case, for N content increasing from 0 up to 0.52, E_U increases from 60 to 215 meV. Equation (9) would yield a fairly linear dependence of E_{04}-E_L on the Urbach energy. The best linear fit (R=0.958) gives a zero intercept a =(0.29$\pm$0.08) eV and a slope $b=(4.95\pm0.52)\times10^{-3}$. However, if we assume reasonable values for N_0 =5 10^{21} $cm^{-3}eV^{-1}$ and R_C=125 Å, as they were found for a-Si:H,[21,18] Eq. (9) predicts $b\approx7.6$. Thus, the experimental data do not agree with the predictions of Dunstain and Boulitrop model, as stated by previous analysis.[8] On the other hand, if we consider a decrease of critical radius R_C with alloying, a sublinear behaviour of E_{04}-E_L vs E_U, at high-N content becomes plausible. In Fig. 8, it is shown that Eq. (9) accounts for the experimental data when a linear decrease of R_C from 125 Å for E_U=60 meV (i.e., for a-Si:H) down to 46 Å for the sample with the higher E_U is considered. Following Eq. (6), such a decrease could be accounted for by a reduction of the radiative lifetime induced by alloying. This reduction is indeed measured, as we will show later.

The topological disorder induced by alloying, reflected in wider tail states, that is in higher E_U, would also explain the weakened temperature quenching of the PL intensity. For all the samples the PL efficiency η versus temperature data are fitted by the semiempirical rule

$$\frac{\eta(T)}{\eta_0}=\frac{1+\chi}{1+\chi\exp\dfrac{T}{T_0}}, \tag{11}$$

where η_0 is the radiative efficiency at low temperature, χ and T_0 are constants depending on the sample composition. It is worth emphasizing that Eq. (11) is consistent with thermal excitation from exponential tails, whose slope is proportional to the factor T_0.[11] T_0 is shown as a function of x in the inset of Fig. 3. The increase of T_0 with x is consistent with the trend of E_U versus composition, in agreement with other results.[7] The increase of η as x increases is due to the large E_U, which reduces the thermal excitation of carriers from tail states to extended states through which carriers diffuse and, eventually, recombine via nonradiative processes. In addition, the carrier diffusion is also reduced by the increase of the Coulomb interaction between electrons and holes due to the decrease of the dielectric constant as x increases.[6]

Carrying on the analysis of the correlation between emission and absorption properties of a-$Si_{1-x}N_x$:H we investigate the recombination kinetics yielded by TRL data.

The presence of broad tail states in the a-$Si_{1-x}N_x$:H alloys, well account for the average lifetime $\overline{\tau}$ dependence on the emission energy E_{em} shown in Fig. 5, where $\overline{\tau}\propto\exp(-E_{em}/\gamma)$. In fact, such a dependence could be explained by the thermalization process through which photogenerated carriers span lower-energy tail states. The thermalization rate is proportional to the density of localized states that are involved in the process. Thus, γ will depend on the slope of the exponential DOS. A sharper DOS profile leads to a smaller γ. Consequently, γ and E_U are strictly correlated. This explains the weaker spectral dependence of the average decay time on emission energy for N-rich samples with respect to the Si-rich ones.

When radiative and nonradiative recombination rates (W_R and W_{NR}, respectively) are competing, η and $\overline{\tau}$ are given by

$$\eta=\frac{W_R}{W_R+W_{NR}}\qquad\overline{\tau}=\frac{1}{W_R+W_{NR}}. \tag{12}$$

Thus, the average radiative lifetime $\tau_R=1/W_R=\overline{\tau}/\eta$. Such a ratio, calculated at $E_{em}=E_L$, is shown in the inset of Fig. 8 as a function of E_U. Alloying reduces the radiative lifetime. This is consistent with the reduced carrier diffusion and enhanced Coulomb interaction that leads to a smaller intrapair separation. In fact, considering radiative tunneling between pairs localized in tail states and separated by a distance r, the radiative lifetime τ_R is given approximately by[11]

$$\tau_R=\tau_{0R}\exp\left(\frac{2r}{R_e}\right), \tag{13}$$

where τ_{0R} is the radiative lifetime for completely overlapping electron and hole wave functions. Increasing x,r reduces and hence τ_R. The τ_R shortening induced by alloying is, in turn, fully consistent with the decrease of R_C above postulated.

V. CONCLUSIONS

We presented optical and PL data for a-$Si_{1-x}N_x$:H samples in a wide compositional range ($0.15\leqslant x\leqslant0.52$). The N incorporation yields a widening of the tail states due to static disorder. Such a feature is responsible of the PL line shape, while electron-phonon coupling appears to be weakly influent and cannot be considered the dominant process as previously stated for a-Si:H. The luminescence decay is also

linked to the DOS shape, in particular the spectral dependence of the lifetimes is a consequence of the widened tail states distribution. The temperature quenching of the luminescence intensity is weakened by the alloying, which is consistent with a widening of the tail states and an increasing Coulomb pair interaction. Such findings are further supported by the trend of the radiative lifetime versus composition, which decreases as the N content increases.

ACKNOWLEDGMENTS

We wish to express our gratitude to C.F. Pirri for helpful discussions and to M. Palma, L. Dal Negro, C. Mazzoleni for technical support. The authors are also indebted to P. Rava for the deposition of a-$Si_{1-x}N_x$:H samples, and they wish to thank the Institute LAMEL-CNR of Bologna, where the PECVD system is installed.

[1] C.E. Morosanu, Thin Solid Films **65**, 171 (1980).
[2] M.J. Powell, B.C. Easton, and O.F. Bill, Appl. Phys. Lett. **48**, 794 (1981).
[3] S.M. Paasche, T. Toyama, H. Okamoto, and Y. Hamakawa, IEEE Trans. Electron Devices **36**, 2895 (1989).
[4] D. Kruangam, W. Boonkosum, and S. Panyakeow, J. Non-Cryst. Solids **164-166**, 809 (1993).
[5] F. Giorgis, C.F. Pirri, C. Vinegoni, and L. Pavesi, J. Lumin. **80**, 423 (1999).
[6] F. Giorgis, C.F. Pirri, and E. Tresso, Thin Solid Films **307**, 298 (1997).
[7] I.G. Austin, W.A. Jackson, T.M. Searle, and P.K. Bath, Philos. Mag. B **52**, 271 (1985).
[8] T.M. Searle and W.A. Jackson, Philos. Mag. B **60**, 237 (1989).
[9] S.V. Deshpande, E. Gulari, S.W. Brown, and S.C. Rand, J. Appl. Phys. **77**, 6534 (1995).
[10] C. Palsule, S. Gangopadhyay, S. Yi, J.M. Shen, H.A. Naseem, S. Kizzar, and F.H.C. Goh, in *Amophous Insulating Thins Films*, edited by J. Kanicki, W.L. Warren, R.A.B. Derine, and M. Matsumuru, MRS Symposia Proceedings No. 284 (Materials Research Society, Pittsburgh, 1993), p 83.
[11] R.A. Street, Adv. Phys. **30**, 593 (1981).
[12] S. Sawada, N. Hamada, and N. Ookubo, Phys. Rev. B **49**, 5236 (1994).
[13] J. Kanicki and W.L. Warren, J. Non-Cryst. Solids **164-166**, 1055 (1993).
[14] H. Fritzsche, Appl. Phys. Lett. **65**, 2824 (1994).
[15] G.D. Cody, T. Tiedje, B. Abeles, B. Brooks, and Y. Goldstein, Phys. Rev. Lett. **47**, 1480 (1981).
[16] J. J. Markham, *F-centres in Alkali Halides* (Academic Press, New York, 1966).
[17] F. Giorgis, Defect Diffus. Forum **134-135**, 33 (1996).
[18] F. Boulitrop and D.J. Dunstan, Phys. Rev. B **28**, 5923 (1983).
[19] D.J. Dunstan and F. Boulitrop, Phys. Rev. B **30**, 5945 (1984).
[20] L. Tessler and I. Solomon, Phys. Rev. B **52**, 10 962 (1995).
[21] L. Ley, in *Properties of Amorphous Silicon and its Alloys*, edited by T. Searle, emis Datareviews Series No. 19-INSPEC (INSPEC IEE, London, UK, 1998), p. 113.